batteries

MDPI

Article

Improvement of Interphase Stability of Hard Carbon for Sodium-Ion Battery by Ionic Liquid Additives

Dexi Meng [1,2], Zongkun Bian [3,*], Kailimai Su [2], Yan Wang [2,4], Zhibin Lu [2], Enlin Cai [1,*] and Junwei Lang [2,4,*]

[1] College of Electronics and Information (Micro-Nano Technology College), Qingdao University, Qingdao 266071, China; mengdexi@qdu.edu.cn
[2] Research Center of Resource Chemistry and Energy Materials, State Key Laboratory of Solid Lubrication, Lanzhou Institute of Chemical Physics, Chinese Academy of Sciences, Lanzhou 730000, China; suklm@licp.cas.cn (K.S.); wangyan@licp.cas.cn (Y.W.); zblu@licp.cas.cn (Z.L.)
[3] School of Materials Science and Engineering, Lanzhou University of Technology, Lanzhou 730050, China
[4] Shandong Laboratory of Advanced Materials and Green Manufacturing at Yantai, Yantai 264000, China
* Correspondence: zongkunbian@gmail.com (Z.B.); caienlin@qdu.edu.cn (E.C.); jwlang@licp.cas.cn (J.L.)

Abstract: Hard carbon (HC), which is one of the anode materials widely used in commercial sodium-ion batteries at present, suffers from a thick and unstable solid electrolyte interface (SEI) layer formed by the self-reduction in traditional carbonate-based electrolytes on its surface. This phenomenon impacts the battery's Coulomb efficiency, cycle stability, and rate performance. In this paper, a pyrrolidinium-type di-cation ionic liquid, butyl-1,4-di(methylpyrrolidinium) di[hexafluorophosphate] (C_4di[mPy].di[PF_6]), is studied as an electrolyte additive to improve the interphase stability of the HC anode. The PF_6^- in C_4di[mPy].di[PF_6] enhances the coordination number between Na^+ and PF_6^-, and C_4di[mPy]$^{2+}$ is preferentially reduced, jointly participating in the construction of stable, thin, dense and NaF-rich SEI films, thus laying the foundation for improving battery performance. As a result, in the carbonate electrolyte containing 2 wt% C_4di[mPy].di[PF_6], the reversible capacity of the HC/Na half-cell is increased by 14.7%, and the capacity retention rate remains at 90.4% after 400 cycles. This work provides reference for future research and design of high-performance ion liquid additives.

Keywords: sodium-ion battery; hard carbon; interphasial stability; solid electrolyte interphase; ionic liquid

check for updates

Academic Editor: Teofilo Rojo

Received: 5 February 2025
Revised: 28 February 2025
Accepted: 6 March 2025
Published: 8 March 2025

Citation: Meng, D.; Bian, Z.; Su, K.; Wang, Y.; Lu, Z.; Cai, E.; Lang, J. Improvement of Interphase Stability of Hard Carbon for Sodium-Ion Battery by Ionic Liquid Additives. *Batteries* **2025**, *11*, 102. https://doi.org/10.3390/batteries11030102

Correction Statement: This article has been republished with a minor change. The change does not affect the scientific content of the article and further details are available within the backmatter of the website version of this article.

Copyright: © 2025 by the authors. Licensee MDPI, Basel, Switzerland. This article is an open access article distributed under the terms and conditions of the Creative Commons Attribution (CC BY) license (https://creativecommons.org/licenses/by/4.0/).

1. Introduction

In the wave of the energy revolution in the 21st century, electrochemical energy storage technology, as a key link to promote the transformation of the energy structure and achieve the popularization of clean energy, has been widely researched around the world [1,2]. As a potential electrochemical energy storage device, the sodium-ion battery has become an important supplement to the lithium battery because of its advantages of abundant resources, low cost and environmental friendliness [3]. In the research and development of sodium-ion batteries, the selection and optimization of anode materials play a crucial role in improving the overall performance of the battery and promoting its commercialization process. Hard carbon (HC), as a promising candidate for sodium-ion battery anode materials, exhibits unique structural and performance features. These features enable it to reversibly intercalate sodium ions and achieve a specific capacity of 250–320 mAh g^{-1}, making it a primary material for commercial sodium-ion batteries [4–8].

However, HC anodes still face several challenges in practical applications, including slow ion transport rates and poor electrode/electrolyte interface stability. In order to alleviate this problem, researchers have improved the structure and properties of HC through methods such as heteroatom doping [9,10] and structural adjustment [11] to improve the electrical conductivity or enhance the stability of carbon materials. However, atomic doping relies on complex synthesis processes, which make it difficult to precisely control the atomic conditions, leading to uneven doping and, consequently, differences in the performance of various parts of the hard carbon material. Furthermore, the complexity of the process increases both the difficulty of material preparation and the cost [12]. In addition to material modification, regulating electrolyte composition or introducing electrolyte additives are also effective ways to improve the stability of the HC anode. Similar to lithium-ion batteries, the electrolyte of sodium-ion batteries not only conducts ions between electrodes, but also forms a solid electrolyte interface (SEI) film on the surface of the anode [13]. However, the SEI film produced by traditional ester solvent-based electrolytes is thick and unstable [14], and ether solvent-based electrolytes will decompose under high pressure [15,16]. The HC/electrolyte interface is unstable, which easily lead to the decomposition of electrolyte and the corrosion of electrode material, thus shortening battery cycle life [17]. The introduction of additives into the electrolyte that can preferentially undergo reduction reactions on the surface of HC can guide the directional growth of the SEI film and alter its thickness, stability, and interface impedance [18,19]. Thus, to enhance the development of SIBs with a long cycle life, it is urgent to develop electrolyte additives that can stabilize the HC anode.

Ionic liquids (ILs) possess unique properties, including a low melting point, high thermal and chemical stability, high ionic conductivity, a wide electrochemical window, non-volatility, and non-flammability, and are an ideal alternative to organic solvents or electrolyte additives for sodium-ion batteries, which can improve the safety, energy/power density, and cycle stability of batteries. ILs can be used alone or as an additive in electrolytes [20,21]. For example, Zhao et al. developed a novel imidazolium-based ILs (AMMEIMTFSI) as an additive (the optimal content is 10 vol%) for carbonate electrolyte to enhance the antioxidant capacity of the electrolyte (withstand 5V) [22]. Luciana et al. used a pyrrole-based ILs ($PYR_{14}FSI$) as the independent solvent to dissolve NaTFSI salt and form IL-based electrolyte. This IL-based electrolyte formed a dense CEI film on the cathode surface, which reduced the dissolution of manganese ions and effectively improved the cycle stability of the cathode material [23]. Atsushi et al. studied the electrochemical characteristics of HC anode in NaFSA-C_1C_3pyrFSA electrolyte, and proved that ILs can promote the insertion/removal of sodium ions and inhibit dendrite growth, thus significantly improving the cycle performance and rate performance of the HC anode [24]. Meng et al. used allylbutylpiperidine-containing ILs (pp14FSI) as an electrolyte additive (the optimal content is 15 vol%) and found that it significantly enhanced the cycling stability and high temperature performance for HC anodes [25]. The above research has shown that designing IL-based electrolytes is an effective strategy to enhance the electrode stability and rate performance of sodium-ion batteries.

Our recent study found that the di-cationic IL (the number of methylene groups that bridge the two cations is 4) has higher electrochemical stability and chemical/physical adsorption compared to ordinary mono-cationic ILs [26,27]. Therefore, in this article, we report a novel di-cationic ILs additive, C_4di[mPy].di[PF_6], for enhancing the cycling stability of HC anode. The introduction of C_4di[mPy].di[PF_6] increases the concentration of PF_6^-, which helps form an NaF-rich SEI film. Additionally, since C_4di[mPy]$^{2+}$ has the lowest LUMO energy level, it could be preferentially reduced, leading to the formation of a stable, thin, and dense SEI film. Based on these effects, the obtained SEI film improved the interface stability of HC anode, reduced the electrolyte–anode material side reactions,

and improved the long-cycle stability of the battery. As a result, the Na||HC half-cell with C_4di[mPy].di[PF_6] showed a capacity retention rate of 90.4% after 400 cycles at 100 mA g^{-1} and 82% after 500 cycles at 300 mA g^{-1}. In addition, the capacity retention rate of the vanadium phosphate sodium (NVP)||HC full cell has also been significantly improved.

2. Experimental Section

2.1. Electrolyte and Electrode Preparations

2.1.1. Electrolyte Preparations

The solute sodium hexafluorophosphate ($NaPF_6$), along with the solvents ethylene carbonate (EC) and dimethyl carbonate (DMC) of battery-grade purity, were purchased from the official website of AnNaiji Reagents. All the above components were used directly without further processing. The two solvents were mixed in a 1:1 volume ratio to prepare an EC/DMC mixed solvent, and $NaPF_6$ was dissolved in the solvent to form a 1M $NaPF_6$/EC:DMC base electrolyte. C_4di[mPy].di[PF_6] at concentrations of 1 wt%, 2 wt%, and 5 wt% was added to the base electrolyte to obtain electrolytes containing additives. The synthesis of C_4di[mPy].di[PF_6] was conducted according to Ref. [26], with the difference that $TFSI^-$ was replaced by $PF_6{}^-$ in the ion exchange procedure. All electrolyte preparation, battery fabrication, and disassembly were carried out in a glove box (MBRAUN, Munich, Germany) filled with argon, with both water and oxygen content below 0.1 ppm.

2.1.2. Electrode Preparation and Coin Cell Fabrication

Electrode: HC was purchased from Kuraray, Japan. The HC, acetylene black (conductive agent), and PVDF (binder) were evenly mixed in a mass ratio of 90:5:5, and then an appropriate amount of N-Methylpyrrolidone (NMP) was added to form a homogeneous slurry. The slurry was evenly coated onto an aluminum foil using a 75 um scraper. Subsequently, the electrode was dried at 110 °C in a vacuum drying oven for 12 h and then cut into circular pieces with a diameter of 12 mm. The positive electrode uses vanadium phosphate sodium (NVP) as the active material. The NVP: Super-P: PVDF were uniformly mixed in a mass ratio of 8:1:1, and the electrode preparation process was similar to that of the negative electrode.

Na||HC half-cell: The half-cell was assembled using Na metal (15.6 mm in diameter) as the counter electrode, glass fiber (Whatman Company) as the separator, and HC electrode as the working electrode.

NVP||Na half-cell: The HC electrode in the Na||HC half-cell was replaced with an NVP electrode.

Na||Na symmetrical cell: The HC electrode in the Na||HC half-cell was replaced with Na metal.

Full cell: The coin-type full cell was assembled with an HC electrode as the negative electrode, an NVP electrode as the positive electrode, and glass fiber as the separator.

Swagelok cell: The Na||HC||Na three-electrode Swagelok cell was assembled to test the battery rate performance, using Na metal as both the counter electrode and the reference electrode, an HC electrode as the working electrode, and glass fiber as the separator.

2.1.3. Electrochemical Measurements

The LAND test system (CT2001A, Wuhan LAND Electronics Ltd., Wuhan, China) was used to perform constant current charge–discharge tests on the Na||HC half-cell, Na||NVP full cell and Na||HC||Na three-electrode cell at 25 °C to investigate their capacity, first coulomb efficiency, rate performance, and cycle stability. Cyclic voltammetry (CV) analysis of the Na||HC half-cell was conducted using an electrochemical workstation (CHI660E, ChenHua, Shanghai, China) with a scan rate of 0.1 mV s^{-1} in the potential range

from 0.01 V to 2.5 V to investigate the oxidation-reduction properties of the electrolyte containing additives. Electrochemical impedance spectroscopy (EIS) was measured at an electrochemical workstation with a frequency range from 0.01 Hz to 100 KHz with an amplitude of 5 mV. The GITT curve of the battery was obtained through intermittent charging or discharging of the battery using the battery test system (BTS-80, NEWARE, Shenzhen, China), and the charging and discharging current density was set at 30 mA g^{-1}.

2.2. Physical Characterization

After the test was completed, the batteries were transferred into the glove box for disassembly, and the electrodes were cleaned with DMC to remove the residual electrolyte on the surface, and then dried in a vacuum oven at 90 °C for 12 h. Scanning electron microscopy (SEM, Thermo Scientific Helios 5 CX, Waltham, MA, USA) and energy dispersive spectroscopy (EDS) were employed to investigate the surface morphology of the original HC electrode and the HC electrode after circulating in different electrolytes, and the elements were qualitatively and quantitatively analyzed. Transmission electron microscopy (TEM, FEI F30, Hillsboro, OR, USA) was employed to observe the microstructure and component of the interfacial layer formed by HC electrode cycling in different electrolytes. The crystal structure of HC was determined utilizing an X-ray diffractometer (XRD, Bruker D8 Advance, Karlsruhe, Germany) equipped with Cu-Kα radiation (λ = 1.5418Å) over a range of 5°~90°. The composition of the SEI layer on the HC electrode was assessed via X-ray photoelectron spectroscopy (XPS, ESCALAB 250, Waltham, MA, USA), employing a monochromatic Al Kα-X-ray source (E = 1468.68 eV). Furthermore, the functional groups of different electrolyte samples were examined using Fourier transform infrared spectrometer (FTIR, NICOLET iS50 FT-IR, Waltham, MA, USA) in the mid-infrared region. The solvation structure of the electrolytes was analyzed by Raman spectroscopy(DXR 2xi, Waltham, MA, USA).

2.3. Theoretical Calculation

The lowest unoccupied molecular orbital (LUMO) and highest occupied molecular orbital (HOMO) energy levels of solvents and additives were calculated by the natural bond orbital method. The distribution states of ions and solvents in the electrolyte (RDF, coordination number) was calculated by classical molecular dynamics (CMD) simulation.

3. Results and Discussion

Figure 1a shows the structural diagram of C_4di[mPy].di[PF_6], where the cation structure is formed by connecting two methylpyrrolidine-cation groups together through an alkyl skeleton. The cation forms an ion pair with two PF_6^- ions through electrostatic interactions, forming a stable ionic liquid. The unique structure of C_4di[mPy].di[PF_6] directly influences the properties of the electrolyte. Firstly, the behavior and function of ILs in electrolytes were analyzed using FTIR spectra and Raman spectra. As shown in Figure 1b, 0% represents 1M $NaPF_6$/EC:DMC (1:1) electrolyte, and 2 wt% ILs represents 1M $NaPF_6$/EC:DMC (1:1) + 2 wt% C_4di[mPy].di[PF_6] electrolyte. It can be seen that the C=O peak in the EC/DMC solvent is relatively sharp. However, in the 0% and 2 wt% electrolyte, the C=O peak becomes broader, especially in the electrolyte containing 2 wt% ILs, which may be affected by the effect of hydrogen bonding. Meanwhile, it can be clearly seen from the IR spectra that after adding IL additives, obvious characteristic peaks appear at 1457 cm^{-1} and 1292 cm^{-1}, corresponding to the -CH_2- bond and C-N bond in C_4di[mPy]$^{2+}$, respectively, indicating that the IL additives have been uniformly dispersed in the electrolyte. Of particular note is that the characteristic peak located at 1292 cm^{-1} has a strong and relatively sharp intensity, indicating the presence of a large number of ionic liquid

ions (N^+) in the electrolyte, which is beneficial for improving the ionic conductivity of the electrolyte. As shown in Figure 1c, it was found that the addition of ILs resulted in a blue shift in the P-F stretching vibration peak at 829 cm^{-1}, which demonstrated an enhanced interaction between Na^+ and PF_6^-. As shown in Figure 1d, in the Raman spectra, after $NaPF_6$ was dissociated in EC/DMC solvent and solvent containing 2 wt% ILs, the P-F peak in PF_6^- shifted from 765 cm^{-1} to 742 cm^{-1} and 745 cm^{-1}, respectively. The displacement of the P-F peak in electrolyte containing 2 wt% ILs is slightly smaller, indicating that there is stronger binding between Na^+ and PF_6^- than that in the electrolyte without ILs [28]. In addition, compared with the spectra of 0% electrolyte and EC/DMC solvent, it was found that the characteristic peak at 895 cm^{-1} undergoes a blue shift after EC/DMC solvent binding with Na^+, indicating that Na^+ and EC/DMC solvent have strong binding force. However, in the electrolyte containing 2 wt% ILs, the characteristic peak at this point shows almost no shift, indicating that the addition of ILs weakens the interaction between Na^+ and EC/DMC solvent. Pure ILs have another characteristic peak at 902 cm^{-1}, but this characteristic peak exhibits a blue shift in the electrolyte containing 2 wt% ILs, indicating a strong interaction between a certain component in the electrolyte and C_4di[mPy].di[PF_6]. From Figure 1e, it can be seen that as the concentration of ILs increases, the red shift of the characteristic peak of EC/DMC solvent at 895 cm^{-1} gradually increases, indicating that the interaction between Na^+ and the EC/DMC gradually decreases. In addition, conductivity tests were carried out on different electrolytes (Figure 1f), and it can be seen that the ionic conductivity of the electrolyte was significantly increased by the addition of C_4di[mPy].di[PF_6]. Because ILs are composed of asymmetric anions and cations, the interaction between the ions is weak, so they can be completely dissociated into free anions and cations in organic solvents, thus enhancing the conductivity of the electrolyte [29,30].

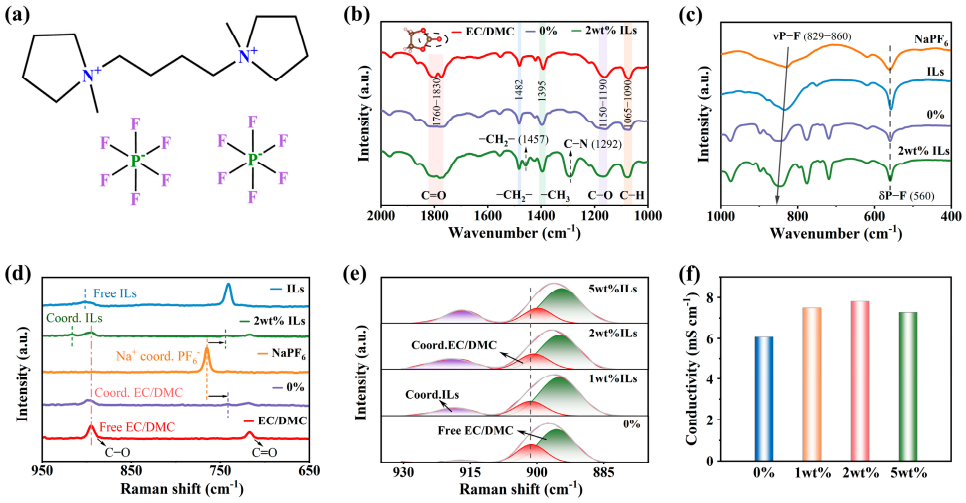


Figure 1. (**a**) The structure of C_4di[mPy].di[PF_6]; (**b**,**c**) FTIR spectra of different electrolytes; (**d**) Raman spectra of different electrolytes and their constituent salts and solvents; (**e**) Raman spectra of different IL electrolytes; (**f**) the ionic conductivity of different IL electrolytes.

As shown in Figure 2a, constant current charge–discharge tests were conducted on Na||HC half-cell using different electrolytes at a current density of 15 mA g^{-1}. The capacity of the HC anode in the base electrolyte was lower and less stable than that in the electrolyte containing ILs. The initial reversible specific capacity of HC anode in electrolyte containing 2 wt% ILs was 14.7% higher than that in the base electrolyte. After 100 cycles, the capacity of the HC anode in electrolytes containing ILs remained above 300 mAh g^{-1}. Figure S5a shows the EIS spectrum and corresponding fitting curve of the Na||HC half-cell after 10 cycles. Compared with the base electrolyte, the SEI impedance

(R_{SEI}) and charge transfer impedance (R_{ct}) of electrolyte containing C_4di[mPy].di[PF_6] are significantly reduced (Figure S5b). Above, by comparing the three electrolytes containing different proportions of additives, it is found that the electrolyte containing 2 wt% ILs has the highest ionic conductivity, the highest capacity and cycling stability, and lowest impedance value. Therefore, the electrolyte additive containing 2 wt% ILs is chosen as the best proportion. Further characterization and discussion will focus on the comparison between the base electrolyte and the electrolyte containing 2 wt% C_4di[mPy].di[PF_6].

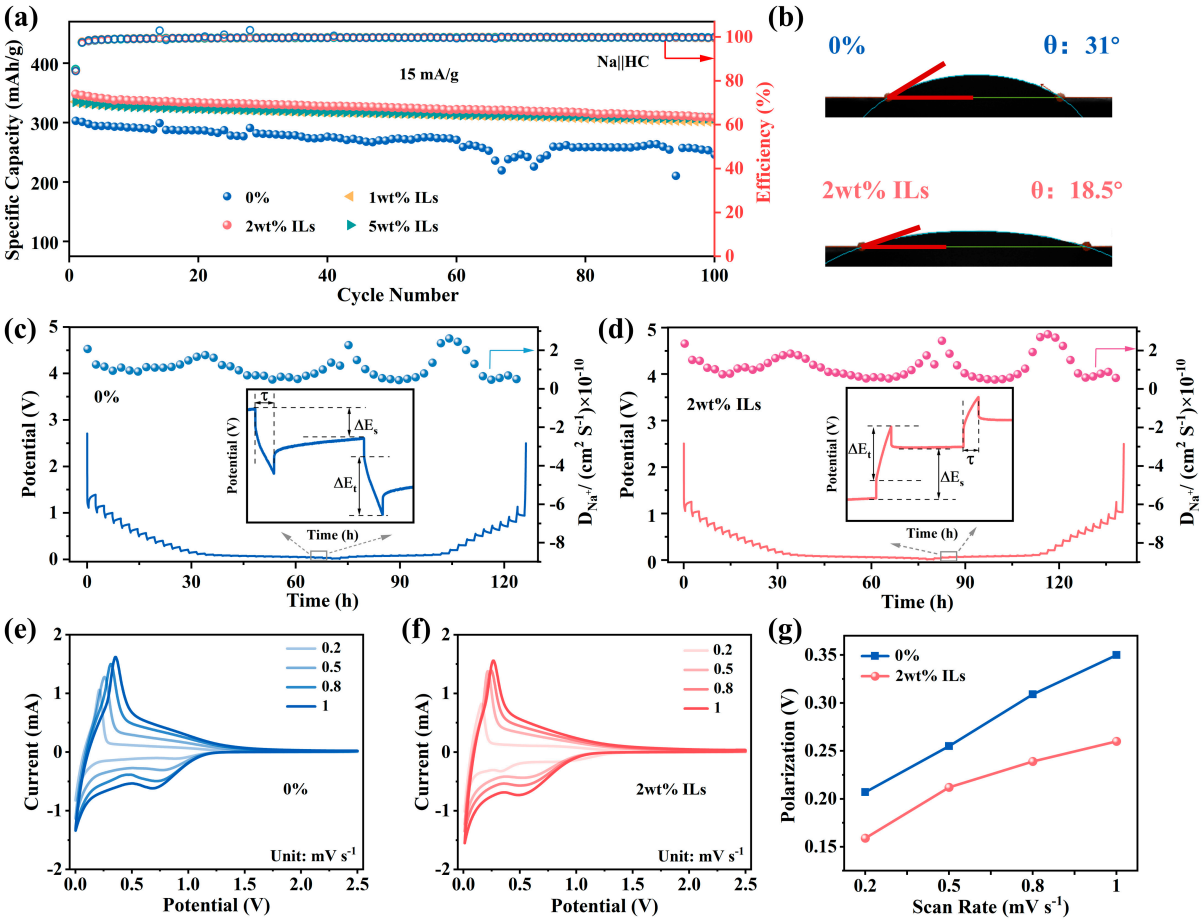


Figure 2. (**a**) The cycling performance of the Na||HC half-cell using different electrolytes at 15 mA g^{-1} for 100 cycles; (**b**) wettability of different electrolytes on HC anode; GITT curves of Na||HC battery using (**c**) base electrolyte and (**d**) electrolyte containing 2 wt% ILs; CV curves of HC anode in (**e**) base electrolyte and (**f**) electrolyte containing 2 wt% ILs at different scan speeds, and (**g**) the corresponding polarization potential.

In order to prove that the introduction of C_4di[mPy].di[PF_6] has a positive effect on HC anode rather than Na tablet, we conducted a comparative study on Na||Na symmetric cells using electrolytes with and without ILs additive, and the results are depicted in Figure S6. It is evident that the C_4di[mPy].di[PF_6] only reduces the polarization degree of the Na||Na symmetric cell, but has little effect on the stability improvement, which proves that the performance improvement of the Na||HC half-cell is due to the enhancement of the stability of the HC anode by the additive. In order to further explore the mechanism of action behind this stability enhancement, an in-depth analysis of the HC anode is necessary. As shown in Figure 2b, the wettability of the base electrolyte and the additive electrolyte to the HC anode were tested. The traditional electrolyte usually faces difficulty in wetting the electrode quickly and evenly, resulting in an increased internal resistance of the battery and affecting the transmission efficiency of sodium ions [31]. It can be seen that the contact angle

of the traditional electrolyte on the surface of HC anode is as high as 31°, and the contact angle only decreased to 28.2° after 10 s of wetting (Figure S7). In contrast, the contact angle of the electrolyte with additives decreased to 14.7° after 10 s of wetting. The decrease in contact angle proves that the addition of ILs improves the wetting of the electrolyte to the HC anode and helps the electrolyte penetrate into HC microstructure better. In order to further evaluate the transport dynamics of Na^+ at the electrode/electrolyte interface, the Na^+ diffusion coefficients during the discharging and charging processes of HC in the two electrolytes were determined using the constant current intermittent titration technique (GITT), and the result is shown in Figures 2c,d and S8. It is evident that the D_{Na+} value in the electrolyte containing C_4di[mPy].di[PF_6] is consistently higher than that in the electrolyte without additives throughout the entire charging and discharging cycle, indicating that the C_4di[mPy].di[PF_6] additive enhanced the Na^+ transfer kinetics and ionic diffusion coefficient. In addition, according to the CV curves (Figure 2e,f) of HC anode obtained at various scan rates in two electrolytes, the corresponding polarization curves were drawn, as shown in Figure 2g. It is observed that the polarization of HC in the electrolyte containing 2 wt% ILs is lower than that in electrolytes without additive, and this difference became more obvious with the increase in the scanning rate, indicating that HC anode has excellent sodium storage kinetics in the electrolyte containing C_4di[mPy].di[PF_6].

In order to comprehensively evaluate the stability of the HC anodes, the cyclic performance of the Na||HC half-cells using base electrolyte and 2 wt% ILs electrolyte were tested first at a low current density of 15 mA g^{-1} for 10 cycles, and then at a current density of 100 mA g^{-1} for 400 cycles. As shown in Figure 3a, the cycling capacity and stability of the HC anode in the base electrolyte were lower compared to those in the electrolyte containing 2 wt% ILs. Figure S9 compares the cycling performance of electrolytes with different ratios of ILs at a current density of 100 mA g^{-1}. It can be seen that the HC anode has a more stable capacity in electrolytes containing 2 wt% and 5 wt% ILs. Figure S10 compares the long-term cycling capacity and efficiency of these two electrolytes. Although the decay trend of the two is similar, the HC anode has better capacity and retention in electrolytes containing 2 wt% ILs, with a retention rate of 90.4% after 400 cycles at 100 mA g^{-1}. By comparing the charge and discharge curves of the HC anode in base electrolyte and in the electrolyte containing 2 wt% ILs (Figure 3c,d), it can be more intuitively observed that the capacity decay rate of HC anode in the base electrolyte is much higher than that of in the electrolyte containing 2 wt% ILs. This phenomenon may occur as a result of the continuous reduction and deposition of the electrolyte on the HC surface, which is related to the destruction and reconstruction of SEI film. The introduction of C_4di[mPy].di[PF_6] enhanced the cycling stability of the HC anode, possibly due to the formation of a relatively stable SEI film, which suppressed the side reactions on the HC surface. In addition, in many fields, batteries often face the challenge of requiring charge and discharge under high current density, so we conducted a long cycle test on the Na||HC half-cell at high current density of 300 mA g^{-1} (Figure S11). The capacity retention rate of HC anode after 500 cycles in the base electrolyte and in the electrolyte containing 2 wt% ILs are 63.8% and 82%, respectively, and the capacity decrease was relatively obvious in the base electrolyte. This result shows that C_4di[mPy].di[PF_6] can also significantly improve the long cycle stability of the battery at high current density.

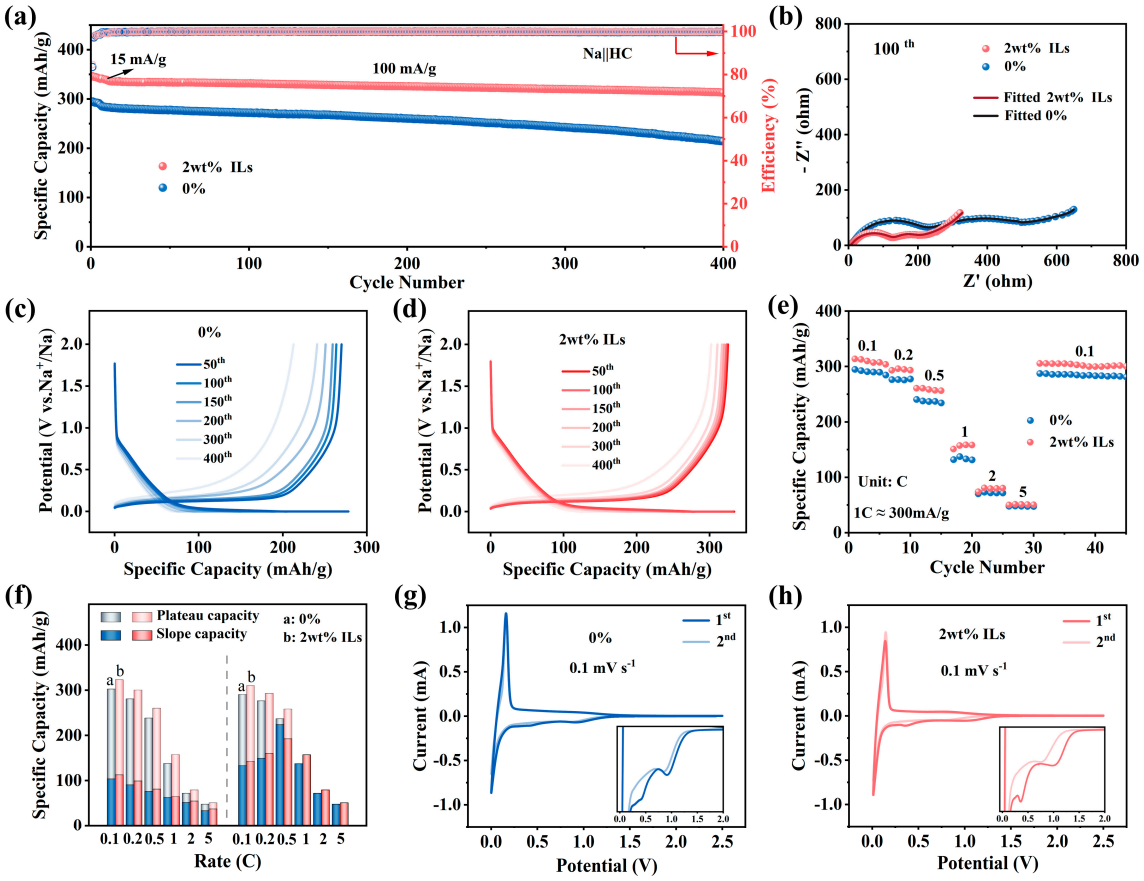


Figure 3. (**a**) Comparison of Na||HC battery cycling between base electrolyte and electrolyte containing 2 wt% ILs at a current density of 100 mA g^{-1}, with (**c**,**d**) corresponding charge–discharge curves; (**b**) Nyquist plots after 100 cycles at 300 mA g^{-1} in different electrolytes; (**e**) rate performance under different electrolytes, and (**f**) the corresponding plateau capacity and slope capacity derived from discharge (left) and charge (right); CV curves of the first 2 cycles at a scan rate of 0.1 mV s^{-1} in (**g**) base electrolyte and (**h**) electrolyte with 2 wt% ILs.

The interface reaction between the electrolyte and HC anode during the cycling process was studied using the EIS test, and the equivalent circuit was fitted to obtain the resistance value (Figure 3b). It can be seen that the SEI resistance (R_{SEI}) and the charge transfer resistance (R_{ct}) values in the electrolyte containing 2 wt% ILs are 113.2 Ω and 28.1 Ω, respectively, which are both lower than those in the base electrolyte (R_{SEI} is 208.5 Ω and R_{ct} is 165 Ω). It can be seen that the charge transfer kinetics of Na^+ in the HC anode in electrolyte containing C_4di[mPy].di[PF_6] are superior to those in the base electrolyte. To more accurately evaluate the rate performance of HC anode in different electrolytes, Figure 3e presents the capacity performance of HC anode tested using a three-electrode system at different current densities. The results indicate that the HC anode in electrolytes containing additive exhibits excellent rate performance when the current density is less than 1C. From Figure 3f, it can be seen that when the current density is less than 0.5C, the HC anode still has a significant plateau (<0.1 V vs. Na^+/Na) capacity in the electrolyte containing additives, indicating that the addition of additives enhances the sodium storage capacity of HC [32]. The plateau capacity decreases significantly with the increase in current density, while the slope capacity remains relatively high. This indicates that the slope capacity has an important effect on the rate performance, which can provide a more stable capacity output at high current density.

In addition to the above electrochemical tests, CV curves can also be used to directly observe the change in redox potential and the reaction reversibility of the electrode ma-

terials during the charge and discharge process, so as to understand the electrochemical characteristics of the HC anode more comprehensively. Figure 3g,h show the CV curves of HC anode at the scan rate of 0.1 mV s^{-1} in the base electrolyte and the electrolyte containing 2 wt% ILs. During the first cathodic scan, both electrolytes exhibit irreversible reduction peaks due to the SEI film formation at approximately 0.91 V and 1.03 V, respectively. The higher reduction potential indicates that the additive was preferentially reduced and participates in the formation of the SEI film [18,33,34]. Furthermore, the CV curves show that the voltage difference between the oxidation peak and the reduction peak in the electrolyte containing additive is smaller than that in the base electrolyte, indicating that the additive can effectively reduce the polarization of the HC material. Figure S12 displays the charge/discharge curves for the first three cycles of HC anode in electrolyte containing 2 wt% ILs and the corresponding differential capacitance curves in the low current of 15 mA g^{-1}. The initial discharge specific capacity of the HC anode in electrolyte containing 2 wt% ILs is 410.8 mAh g^{-1}, and the initial charge specific capacity is 348 mAh g^{-1}, with an initial coulombic efficiency of 84.75%. In contrast, the initial discharge specific capacity of the HC anode in the base electrolyte is 358.9 mAh g^{-1}, while the initial charge specific capacity is 303 mAh g^{-1} and the initial coulombic efficiency of 84.5% (Figure S13). The HC anode in both electrolytes exhibited a large irreversible capacity, indicating that significant irreversible reactions occurred during this period, mainly resulting from SEI film formation. During the subsequent cycling process, the irreversible capacity significantly decreased. Meanwhile, the conclusion drawn from the differential capacitance curve is similar to that of the CV curve mentioned above. In the 2 wt% ILs electrolyte, an irreversible reduction peak of HC anode appeared at approximately 1.05 V during the first discharge process.

As shown in Figure 4a–c, the morphologies of the original HC anode, the HC anode tested after 20 cycles in the base electrolyte and the electrolyte containing 2 wt% C_4di[mPy].di[PF_6] were characterized using SEM. The original electrode shows sharp edges and a smooth surface, as depicted in Figure 4a. It is evident that the surface of the cycled HC anode exhibits a distinct layer of deposition compared to the uncycled anode. These deposits are composed of the decomposition products from sodium salts and from organic solvents and are usually divided into two layers, with an outer layer of organic material and an inner layer of inorganic compounds [35]. In addition, after cycling in the base electrolyte, the HC anode demonstrates a rough surface with uneven depressions, indicating that its original morphology was destroyed. In contrast, the morphology of the HC anode after cycled in electrolyte containing 2 wt% C_4di[mPy].di[PF_6] is very close to its original form, and the edge remains sharp, indicating that C_4di[mPy].di[PF_6] can effectively inhibit side reactions and enhance interface stability. Furthermore, TEM analysis was conducted on the HC anode after cycling in electrolytes with and without the C_4di[mPy].di[PF_6] additive, as depicted in Figures 4d,e and S14. In the absence of additive in electrolyte, significant cracks (Figure S14a) and an uneven SEI film (Figure 4d) can be observed in HC anode, which is also responsible for the rapid attenuation of the capacity. In the presence of 2 wt% C_4di[mPy].di[PF_6] in the electrolyte, the cycled HC anode (Figure S14b) exhibited excellent structural integrity and a uniform and thin SEI film (Figure 4e). Compared with Figure S14c,d, it can be seen that after testing in the electrolyte containing additives, part of the lattice spacing of HC materials decreases, indicating that the addition of additives can inhibit the lattice expansion of HC, thus improving the structural stability and anti-degradation capability of the battery [36].

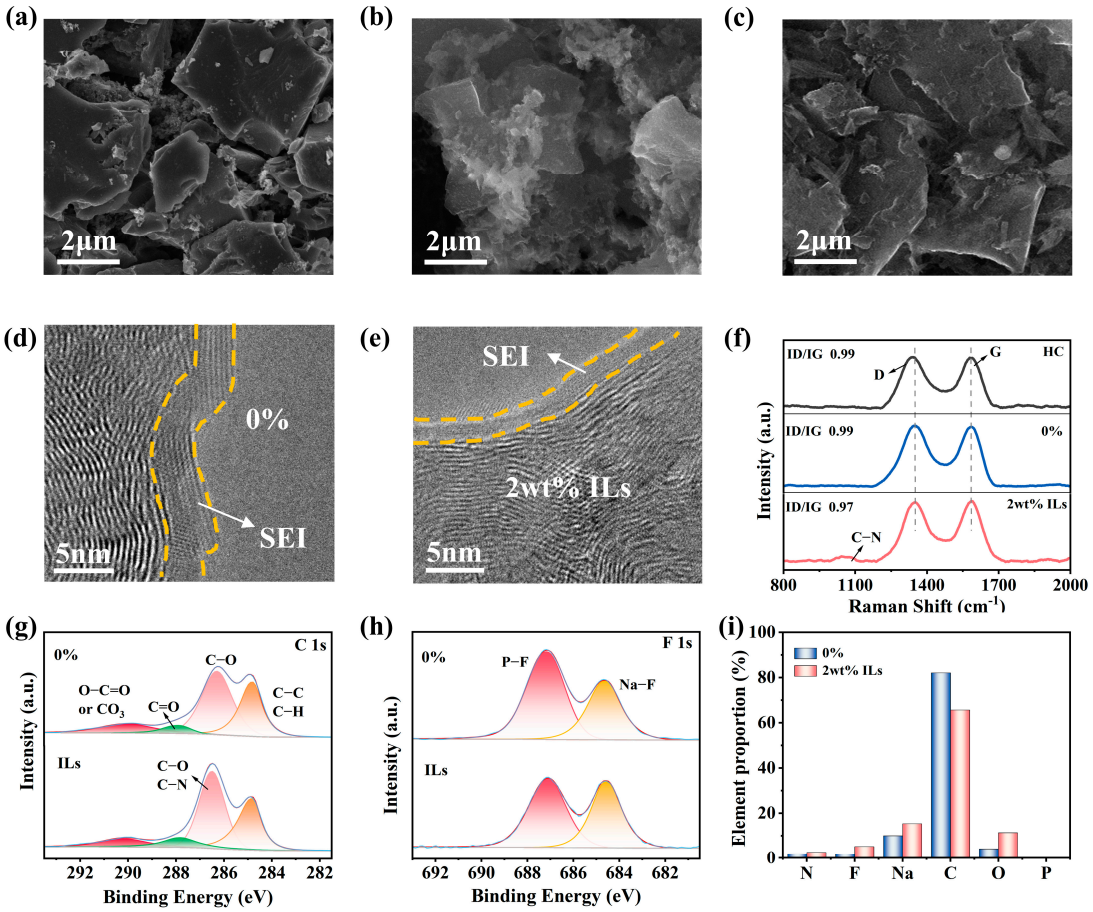


Figure 4. SEM images of (**a**) the original HC anode and HC anode after tested 20 cycles at 0.3 A g^{-1} in (**b**) base electrolyte and (**c**) electrolyte containing 2 wt% ILs; TEM images of the HC anode after tested 20 cycles at 0.3 A g^{-1} in (**d**) base electrolyte and (**e**) electrolyte containing 2 wt% ILs; (**f**) Raman spectra of original HC anode and HC anode after cycling in different electrolytes; XPS spectra of (**g**) C1s and (**h**) F1s of the HC anode after cycling in the base electrolyte and the electrolyte containing 2 wt% ILs; (**i**) element proportion of HC anode after cycling in base electrolyte and electrolyte containing 2 wt% ILs.

The fine spectra of C1s, F1s, and O1s (Figures 4g,h and S15) on the HC anode after cycling were characterized by XPS. The peaks at 284.8 eV (C-C), 286.2 eV (C-O), and 287.9 eV (C=O) in C1s spectrum, as well as the peak at 531.3 eV (RCOO-Na) in O1s spectrum, are primarily associated with organic compounds generated through solvent reduction. The peaks at 289.9 eV (O-CO or CO_3) in the C1s spectrum and the peaks at 684.6 eV (Na-F) and 687.1 eV (P-F) in the F1s spectrum are associated with the inorganic products formed from the decomposition of $NaPF_6$ or PF_6^-. It can be seen that after adding the additive, the peak intensity of Na-F increases, indicating that this SEI is rich in NaF. The TEM-mapping analysis results in Figure 4i showed that the addition of additive increased the content of F and Na elements, which further proved the formation of SEI films rich in NaF. The SEI film rich in NaF can provide a stable protective layer, reduce resistance, improve interface stability, suppress side reactions, and effectively promote the performance improvement of the HC anode [37,38]. By comparing the C1s spectrum in Figure 4g, it can be seen that the addition of ILs increases the binding energy of the C-O/C-N peak, which may be due to the interaction of N in the ILs with surrounding atoms to change the chemical environment. The Raman characterization of the original HC anode and the HC anode after being tested for 20 cycles in the base electrolyte and the electrolyte containing 2 wt% ILs is shown in Figure 4f. The ID/IG ratio slightly decreased after the addition of ILs,

indicating a slight improvement in the structural orderliness of the carbon material. And after the addition of ILs, a new C-N peak was formed [39,40], indicating the presence of nitrogen-containing compounds on the surface of the electrode or SEI film, which come from the N in C_4di[mPy]$^{2+}$. In addition, TEM-mapping (Figures 4i, S16 and S17) showed an increase in N content after the addition of ILs, indicating that C_4di[mPy]$^{2+}$ participated in the reaction.

The solvation structure of 1M $NaPF_6$/EC:DMC (1:1) and 1M $NaPF_6$/EC:DMC (1:1) + 2 wt% C_4di[mPy].di[PF_6] electrolytes was studied by classical molecular dynamics (MD) simulation. From the radial distribution function diagrams of Na^+ (Figure 5a–c), it can be seen that in the electrolyte containing additives, the coordination number n(Na-F) between Na^+ and F atoms increases, while the coordination number n(Na-O_{EC}) between Na^+ and O atoms (in EC) decreases, compared with the base electrolyte. In addition, from Figure 5c, it can be seen that the coordination number n(Na-O_{DMC}) between Na^+ and O atoms (in DMC) slightly increases, while in the first solvation layer, the coordination number n(Na-O_{DMC}) between Na^+ and single-bonded O atoms slightly decreases (Figure S18). Since the coordination of Na^+ is primarily with double-bonded O atoms, the overall trend will not be significantly affected. The sharp peak height of the Na-F(PF_6^-) radial distribution function increases after C_4di[mPy].di[PF_6] addition, and the higher Na-F coordination number in the solvated sheath indicates that more F atoms can migrate to the anode surface and participate in the formation of NaF-rich SEI layer [41,42]. Meanwhile, the coordination number of Na^+ with O atoms in the solvent decreases, indicating a reduction in the interaction between the Na^+ and solvent molecules in the additive electrolyte.

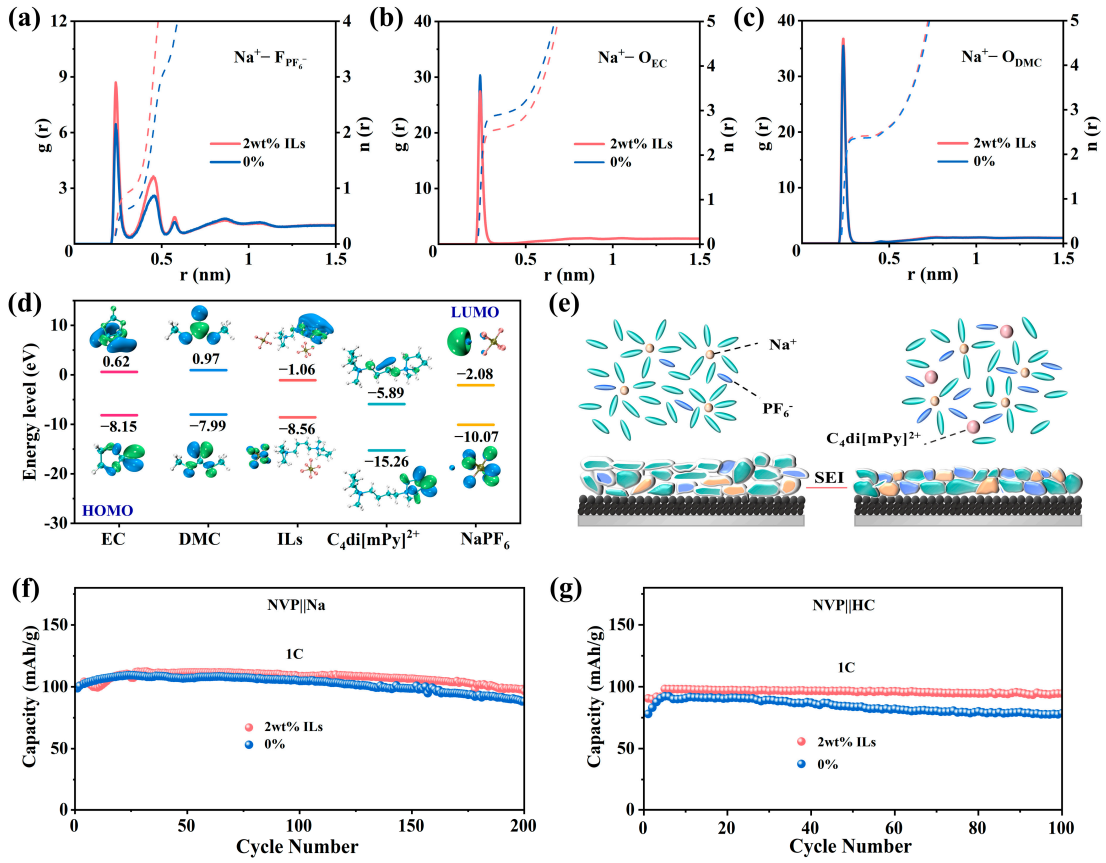


Figure 5. (**a**–**c**) RDFs and CNs of the base electrolyte and the electrolyte containing 2 wt% ILs; (**d**) molecular orbital energy levels of EC, DMC, C_4di[mPy].di[PF_6], $NaPF_6$, and C_4di[mPy]$^{2+}$; (**e**) schematic diagram of the mechanism of action of C_4di[mPy].di[PF_6] additive. Comparison of the performance between (**f**) NVP||Na cell and (**g**) NVP||HC cell at 1C rate.

The frontier orbital energy levels of $NaPF_6$, various solvents, additive molecules and ions calculated by density functional theory (DFT) are illustrated in Figure 5d. According to the frontier orbital theory, the ability of the electrolyte component to participate in oxidation-reduction reactions depends to some extent on the energy levels of its highest occupied molecular orbital (HOMO) and lowest unoccupied molecular orbital (LUMO). The results show that C_4di[mPy]$^{2+}$ has the lowest HOMO and LUMO levels, indicating that it has high oxidation stability and poor reduction stability, and can be preferentially reduced to participate in the construction of SEI film (lower LUMO value indicates a greater electron-accepting ability) [22,43]. The mechanism of action of the C_4di[mPy].di[PF_6] additive is shown in Figure 5e. First, the addition of IL increases the concentration of PF_6^- and the coordination number n(Na-F) between Na^+ and F atom. An increase in the number of PF_6^- in the Na^+ solvated shell will allow more PF_6^- to participate in the reduction reaction in the electrolyte. On the electrode surface, PF_6^- decomposes to produce more F^-, which participates in the formation of a NaF-rich SEI film. Secondly, C_4di[mPy]$^{2+}$ has the lowest LUMO energy level and is preferentially reduced to form a stable, thin, and dense SEI film. Therefore, the PF_6^- and C_4di[mPy]$^{2+}$ work together to improve the cycle life of the HC anode.

Figure 5f shows the cycling performance of the NVP||Na half-cell. It can be seen that the capacity difference between the base electrolyte and the electrolyte containing 2 wt% ILs is not significant, and both remain relatively stable. In the case of the NVP||HC full cell (Figure 5g), the capacity of the cell in two electrolytes remains relatively stable in the early stages of cycling. After 30 cycles, the capacity of the NVP||HC cell in the base electrolyte begins to decline. However, after adding the C_4di[mPy].di[PF_6], thanks to the stability improvement of the HC anode, the capacity retention of the NVP||HC full cell is also significantly increased. This can primarily be attributed to the enhanced stability of the SEI film, which effectively reduces the corrosion and oxidation of the HC anode and extending the battery's lifespan.

4. Conclusions

In conclusion, C_4di[mPy].di[PF_6] was used as the additive for carbonate electrolyte, and its effect on the electrochemical performance of the Na||HC half-cell, NVP||Na half-cell and NVP||HC full cell was systematically studied. Compared with the EC/DMC electrolyte, the EC/DMC + 2 wt% C_4di[mPy].di[PF_6] electrolyte not only improves the migration ability of Na^+, but also promotes the construction of a dense and homogeneous SEI film with abundant NaF. As a result, the capacity retention of the Na||HC half-cell reached 90.4% after 400 cycles at 100 mA g^{-1}, and 82% after 500 cycles at 300 mA g^{-1}. Moreover, the cycling stability of the NVP||HC full cell was also improved. In view of the above beneficial results, we will further increase the in-depth research of ILs additives in the field of sodium-ion batteries.

Supplementary Materials: The following supporting information can be downloaded at: https://www.mdpi.com/article/10.3390/batteries11030102/s1, XRD of HC material; FTIR spectra of solvents and additive electrolytes; wettability of different ILs; cycle life of batteries with different ILs additives; TEM, XPS and TEM-mapping of electrode sheets after cycling in different electrolytes; RDFs and CNs of O atoms in the first solvation shell of DMC. References [5,44–51] are cited in the supplementary materials.

Author Contributions: Writing—original draft, D.M.; writing—review and editing, D.M. and J.L.; conceptualization, Y.W. and J.L.; methodology, Y.W.; software, Z.L.; formal analysis, D.M. and Y.W.; investigation, Z.B. and K.S.; resources, J.L.; supervision, E.C. All authors have read and agreed to the published version of the manuscript.

Funding: This work was supported by the Taishan Scholars Program (No. tsqnz20230629); the Science Fund of Shandong Laboratory of Yantai Advanced Materials and Green Manufacturing (AMGM2022A02, AMGM2023A04); the Chinese Academy of Sciences Western Young Scholars Foundation; the Collaborative Innovation Alliance Fund for Young Science and Technology Workers (HZJJ23-5); and the Excellent Doctoral Project of the Natural Science Foundation of Gansu (24JRRA070); the Joint Fund of the Yulin University and the Dalian National Laboratory for Clean Energy (Grant. YLU-DNL. Fund 2023005).

Data Availability Statement: The data presented in this study are included in the article and its Supplementary Materials.

Conflicts of Interest: The authors declare that this study was conducted in the absence of any financial or commercial relationships that might create potential conflicts of interest.

References

1. Zhang, W.; Lu, J.; Guo, Z. Challenges and future perspectives on sodium and potassium ion batteries for grid-scale energy storage. *Mater. Today* **2021**, *50*, 400–417. [CrossRef]
2. Gu, D. Dedication to Clean Power and Promotion of the Energy Revolution. *Engineering* **2020**, *6*, 1331–1332. [CrossRef]
3. Wang, Y.; Wang, Y.; Wang, Y.-X.; Feng, X.; Chen, W.; Ai, X.; Yang, H.; Cao, Y. Developments and Perspectives on Emerging High-Energy-Density Sodium-Metal Batteries. *Chem* **2019**, *5*, 2547–2570. [CrossRef]
4. Dong, R.; Wu, F.; Bai, Y.; Wu, C. Sodium Storage Mechanism and Optimization Strategies for Hard Carbon Anode of Sodium Ion Batteries. *Acta Chim. Sin.* **2021**, *79*, 1461–1476. [CrossRef]
5. Wang, Q.; Zhu, X.; Liu, Y.; Fang, Y.; Zhou, X.; Bao, J. Rice husk-derived hard carbons as high-performance anode materials for sodium-ion batteries. *Carbon* **2018**, *127*, 658–666. [CrossRef]
6. Zheng, J.; Wu, Y.; Guan, C.; Wang, D.; Lai, Y.; Li, J.; Yang, F.; Li, S.; Zhang, Z. Lignin-derived hard carbon anode with a robust solid electrolyte interphase for boosted sodium storage performance. *Carbon Energy* **2024**, *6*, e538. [CrossRef]
7. Izanzar, I.; Dahbi, M.; Kiso, M.; Doubaji, S.; Komaba, S.; Saadoune, I. Hard carbons issued from date palm as efficient anode materials for sodium-ion batteries. *Carbon* **2018**, *137*, 165–173. [CrossRef]
8. Au, H.; Alptekin, H.; Jensen, A.C.S.; Olsson, E.; O'Keefe, C.A.; Smith, T.; Crespo-Ribadeneyra, M.; Headen, T.F.; Grey, C.P.; Cai, Q.; et al. A revised mechanistic model for sodium insertion in hard carbons. *Energy Environ. Sci.* **2020**, *13*, 3469–3479. [CrossRef]
9. Sun, J.; Sun, Y.; Oh, J.A.S.; Gu, Q.; Zheng, W.; Goh, M.; Zeng, K.; Cheng, Y.; Lu, L. Insight into the structure-capacity relationship in biomass derived carbon for high-performance sodium-ion batteries. *J. Energy Chem.* **2021**, *62*, 497–504. [CrossRef]
10. Chen, F.; Di, Y.; Su, Q.; Xu, D.; Zhang, Y.; Zhou, S.; Liang, S.; Cao, X.; Pan, A. Vanadium-modified hard carbon spheres with sufficient pseudographitic domains as high-performance anode for sodium-ion batteries. *Carbon Energy* **2022**, *5*, e191. [CrossRef]
11. Dong, S.; He, X.; Zhang, H.; Xie, X.; Yu, M.; Yu, C.; Xiao, N.; Qiu, J. Surface modification of biomass-derived hard carbon by grafting porous carbon nanosheets for high-performance supercapacitors. *J. Mater. Chem. A* **2018**, *6*, 15954–15960. [CrossRef]
12. Zhao, Y.; Yang, C.; Yu, Y. A review on covalent organic frameworks for rechargeable zinc-ion batteries. *Chin. Chem. Lett.* **2024**, *35*, 108865. [CrossRef]
13. Li, X.; Yan, P.; Engelhard, M.H.; Crawford, A.J.; Viswanathan, V.V.; Wang, C.; Liu, J.; Sprenkle, V.L. The importance of solid electrolyte interphase formation for long cycle stability full-cell Na-ion batteries. *Nano Energy* **2016**, *27*, 664–672. [CrossRef]
14. Liang, Y.; Song, N.; Zhang, Z.; Chen, W.; Feng, J.; Xi, B.; Xiong, S. Integrating Bi@C Nanospheres in Porous Hard Carbon Frameworks for Ultrafast Sodium Storage. *Adv. Mater.* **2022**, *34*, 2202673. [CrossRef]
15. Dong, R.; Zheng, L.; Bai, Y.; Ni, Q.; Li, Y.; Wu, F.; Ren, H.; Wu, C. Elucidating the Mechanism of Fast Na Storage Kinetics in Ether Electrolytes for Hard Carbon Anodes. *Adv. Mater.* **2021**, *33*, 2008810. [CrossRef]
16. He, Y.; Bai, P.; Gao, S.; Xu, Y. Marriage of an Ether-Based Electrolyte with Hard Carbon Anodes Creates Superior Sodium-Ion Batteries with High Mass Loading. *ACS Appl. Mater. Interfaces* **2018**, *10*, 41380–41388. [CrossRef]
17. Muñoz-Márquez, M.Á.; Saurel, D.; Gómez-Cámer, J.L.; Casas-Cabanas, M.; Castillo-Martinez, E.; Rojo, T. Na-Ion Batteries for Large Scale Applications: A Review on Anode Materials and Solid Electrolyte Interphase Formation. *Adv. Energy Mater.* **2017**, *7*, 1700463. [CrossRef]
18. Zhao, H.; Qi, J.; Tang, X.; Zhang, K.; Teng, J.; Ding, H.; Tao, Q.; Li, J. Effect of crown ether additive on the compatibility of electrolyte and hard carbon anode in sodium ion battery. *J. Alloys Compd.* **2023**, *948*, 169823. [CrossRef]
19. Kim, D.-H.; Kang, B.; Lee, H. Comparative study of fluoroethylene carbonate and succinic anhydride as electrolyte additive for hard carbon anodes of Na-ion batteries. *J. Power Sources* **2019**, *423*, 137–143. [CrossRef]
20. Song, B.; Xiong, X.; Peng, Y.; Liu, X.; Gao, W.; Wang, T.; Wang, F.; Ma, Y.; Zhong, Y.; Cheng, X.-B.; et al. Review of Electrolyte Additives for Secondary Sodium Batteries. *Adv. Energy Mater.* **2024**, *14*, 2401407. [CrossRef]

21. Rangasamy, V.S.; Thayumanasundaram, S.; Locquet, J.-P. Ionic liquid electrolytes based on sulfonium cation for lithium rechargeable batteries. *Electrochim. Acta* **2019**, *328*, 135133. [CrossRef]
22. Zhao, Y. The Study on New Midazolium Ionic Liquidas Electrolyte Additives for Lithium Ion Battery. Master's Thesis, Hebei University of Technology, Tianjin, China, 2020. [CrossRef]
23. Chagas, L.G.; Buchholz, D.; Wu, L.; Vortmann, B.; Passerini, S. Unexpected performance of layered sodium-ion cathode material in ionic liquid-based electrolyte. *J. Power Sources* **2014**, *247*, 377–383. [CrossRef]
24. Fukunaga, A.; Nohira, T.; Hagiwara, R.; Numata, K.; Itani, E.; Sakai, S.; Nitta, K.; Inazawa, S. A safe and high-rate negative electrode for sodium-ion batteries: Hard carbon in NaFSA-C1C3pyrFSA ionic liquid at 363 K. *J. Power Sources* **2014**, *246*, 387–391. [CrossRef]
25. Meng, J.; Jia, G.; Yang, H.; Tang, F.; Peng, Z.; Li, J.; Wang, M. High Temperature Performance Study of Piperidine-based Ionic Liquids in Sodium Ion Batteries. *J. Salt Lake Res.* **2024**, *32*, 46–51. [CrossRef]
26. Xue, K.; Zheng, Z.; Su, K.; Zhang, X.; Wang, Y.; Lang, J. Enhancing stability in Acetonitrile-Based Supercapacitors: Implementation of Di-Pyrrolidinium ionic salts. *Chem. Eng. J.* **2024**, *491*, 152090. [CrossRef]
27. Xue, K.; Zhang, X.; Sun, X.; Su, K.; Wang, Y.; Lang, J.; Zheng, Z. Di-imidazolium ionic liquid based electrolytes for high voltage electrochemical double layer capacitors. *J. Energy Storage* **2024**, *83*, 110473. [CrossRef]
28. Weng, S.; Zhang, X.; Yang, G.; Zhang, S.; Ma, B.; Liu, Q.; Liu, Y.; Peng, C.; Chen, H.; Yu, H.; et al. Temperature-dependent interphase formation and Li+ transport in lithium metal batteries. *Nat. Commun.* **2023**, *14*, 4474. [CrossRef] [PubMed]
29. Pires, J.; Timperman, L.; Jacquemin, J.; Balducci, A.; Anouti, M. Density, conductivity, viscosity, and excess properties of (pyrrolidinium nitrate-based Protic Ionic Liquid+propylene carbonate) binary mixture. *J. Chem. Thermodyn.* **2013**, *59*, 10–19. [CrossRef]
30. Do, M.P.; Bucher, N.; Nagasubramanian, A.; Markovits, I.; Bingbing, T.; Fischer, P.J.; Loh, K.P.; Kühn, F.E.; Srinivasan, M. Effect of Conducting Salts in Ionic Liquid Electrolytes for Enhanced Cyclability of Sodium-Ion Batteries. *ACS Appl. Mater. Interfaces* **2019**, *11*, 23972–23981. [CrossRef]
31. Li, C.; Liang, Z.; Wang, L.; Cao, D.; Yin, Y.-C.; Zuo, D.; Chang, J.; Wang, J.; Liu, K.; Li, X.; et al. Superwettable Electrolyte Engineering for Fast Charging Li-Ion Batteries. *ACS Energy Lett.* **2024**, *9*, 1295–1304. [CrossRef]
32. Ji, X.; Wei, Y.; Yang, H.; Lu, Z.; Jin, S.; Jin, H.; Kong, X.; Ji, H. Extended Plateau Capacity of Hard Carbon Anode for High Energy Lithium-Ion Batteries. *Small* **2024**, *20*, 2402616. [CrossRef] [PubMed]
33. Zhang, W.; Zeng, F.; Huang, H.; Yu, Y.; Xu, M.; Xing, L.; Li, W. Enhanced interphasial stability of hard carbon for sodium-ion battery via film-forming electrolyte additive. *Nano Res.* **2022**, *16*, 3823–3831. [CrossRef]
34. Che, H.; Liu, J.; Wang, H.; Wang, X.; Zhang, S.S.; Liao, X.-Z.; Ma, Z.-F. Rubidium and cesium ions as electrolyte additive for improving performance of hard carbon anode in sodium-ion battery. *Electrochem. Commun.* **2017**, *83*, 20–23. [CrossRef]
35. Zhang, Q.; Pan, J.; Lu, P.; Liu, Z.; Verbrugge, M.W.; Sheldon, B.W.; Cheng, Y.-T.; Qi, Y.; Xiao, X. Synergetic Effects of Inorganic Components in Solid Electrolyte Interphase on High Cycle Efficiency of Lithium Ion Batteries. *Nano Lett.* **2016**, *16*, 2011–2016. [CrossRef] [PubMed]
36. Bian, X.; Dong, Y.; Zhao, D.; Ma, X.; Qiu, M.; Xu, J.; Jiao, L.; Cheng, F.; Zhang, N. Microsized Antimony as a Stable Anode in Fluoroethylene Carbonate Containing Electrolytes for Rechargeable Lithium-/Sodium-Ion Batteries. *ACS Appl. Mater. Interfaces* **2019**, *12*, 3554–3562. [CrossRef]
37. Ma, L.A.; Naylor, A.J.; Nyholm, L.; Younesi, R. Strategies for Mitigating Dissolution of Solid Electrolyte Interphases in Sodium-Ion Batteries. *Angew. Chem. Int. Ed.* **2021**, *60*, 4855–4863. [CrossRef] [PubMed]
38. Yuan, H.; Ma, F.; Wei, X.; Lan, J.L.; Liu, Y.; Yu, Y.; Yang, X.; Park, H.S. Ionic-Conducting and Robust Multilayered Solid Electrolyte Interphases for Greatly Improved Rate and Cycling Capabilities of Sodium Ion Full Cells. *Adv. Energy Mater.* **2020**, *10*, 2001418. [CrossRef]
39. Xu, M.; Wu, F.; Zhang, Y.; Yao, Y.; Zhu, G.; Li, X.; Chen, L.; Jia, G.; Wu, X.; Huang, Y.; et al. Kinetically matched C–N coupling toward efficient urea electrosynthesis enabled on copper single-atom alloy. *Nat. Commun.* **2023**, *14*, 6994. [CrossRef]
40. Wei, J.; Xia, D.; Wei, Y.; Zhu, X.; Li, J.; Gan, L. Probing the Oxygen Reduction Reaction Intermediates and Dynamic Active Site Structures of Molecular and Pyrolyzed Fe–N–C Electrocatalysts by In Situ Raman Spectroscopy. *ACS Catal.* **2022**, *12*, 7811–7820. [CrossRef]
41. Haghkhah, H.; Ghalami Choobar, B.; Amjad-Iranagh, S. Effect of salt concentration on properties of mixed carbonate-based electrolyte for Li-ion batteries: A molecular dynamics simulation study. *J. Mol. Model.* **2020**, *26*, 220. [CrossRef]
42. Lan, X.; Yang, S.; Meng, T.; Zhang, C.; Hu, X. A Multifunctional Electrolyte Additive With Solvation Structure Regulation and Electrode/Electrolyte Interface Manipulation Enabling High-Performance Li-Ion Batteries in Wide Temperature Range. *Adv. Energy Mater.* **2023**, *13*, 2203449. [CrossRef]
43. Ren, Q.; Wang, Q.; Li, Y.; Song, X.; Shangguan, X.; Li, F. High Voltage Electrolytes for Lithium Batteries. *Prog. Chem.* **2023**, *35*, 1077–1096. [CrossRef]

44. Abraham, M.J.; Murtola, T.; Schulz, R.; Páll, S.; Smith, J.C.; Hess, B.; Lindahl, E. GROMACS: High performance molecular simulations through multi-level parallelism from laptops to supercomputers. *SoftwareX* **2015**, *1–2*, 19–25. [CrossRef]
45. Hess, B.; Kutzner, C.; Spoel, D.v.d.; Lindahl, E. GROMACS 4: Algorithms for Highly Efficient, Load-Balanced, and Scalable Molecular Simulation. *J. Chem. Theory Comput.* **2008**, *4*, 435–447. [CrossRef]
46. Berendsen, H.J.C.; Postma, J.P.M.; van Gunsteren, W.F.; DiNola, A.; Haak, J.R. Molecular dynamics with coupling to an external bath. *J. Chem. Phys.* **1984**, *81*, 3684–3690. [CrossRef]
47. York, D.M.; Darden, T.A.; Pedersen, L.G. The effect of long-range electrostatic interactions in simulations of macromolecular crystals: A comparison of the Ewald and truncated list methods. *J. Chem. Phys.* **1993**, *99*, 8345–8348. [CrossRef]
48. Hess, B.; Bekker, H.; Berendsen, H.J.C.; Fraaije, J.G.E.M. LINCS: A linear constraint solver for molecular simulations. *J. Comput. Chem.* **1997**, *18*, 1463–1472. [CrossRef]
49. Silva, A.W.S.d.; Vranken, W.F. ACPYPE-Antechamber python parser interface. *BMC Res. Notes* **2012**, *5*, 367. [CrossRef]
50. Li, Z.L.; Li, W.T.; Zhang, C.; Liu, W.; Peng, J.; An, S.L.; Qiu, X.P. Effect of Electrolyte on the Hard Carbon Anode of Sodium Ion Battery. *Telecom Power Technology.* **2020**, *37*, 40–45. [CrossRef]
51. Su, K.; Chen, J.; Zhang, X.; Feng, J.; Xu, Y.; Pu, Y.; Wang, C.; Ma, P.; Wang, Y.; Lang, J. Inhibition of zinc dendrites by dopamine modified hexagonal boron nitride electrolyte additive for zinc-ion batteries. *J. Power Sources* **2022**, *548*, 232074. [CrossRef]

Disclaimer/Publisher's Note: The statements, opinions and data contained in all publications are solely those of the individual author(s) and contributor(s) and not of MDPI and/or the editor(s). MDPI and/or the editor(s) disclaim responsibility for any injury to people or property resulting from any ideas, methods, instructions or products referred to in the content.